

Stability and magnetism of FeN high-pressure phase with a NiAs-type  
structure.

*Supplement materials.*

Alexey Kartsev

*Computing Center FEB RAS, Khabarovsk, Russia  
National Research Tomsk State University,  
36, Lenina pr., Tomsk, 634050, Russia and  
School of Mathematics and Physics, Queens University Belfast,  
Belfast BT7 1NN, northern Ireland, United Kingdom*

Oleg Feya

*Moscow Institute of Physics and Technology,  
Dolgoprudny, Moscow Region 141700, Russia*

Nina Bondarenko

*Condensed Matter Theory Group, Physics Department,  
Uppsala University, S-751 21 Uppsala, Sweden*

Alexander G. Kvashnin

*Skolkovo Institute of Science and Technology,  
3 Nobel St., Moscow 143026, Russia and  
Moscow Institute of Physics and Technology,  
Dolgoprudny, Moscow Region 141700, Russia*

(Dated: February 1, 2019)

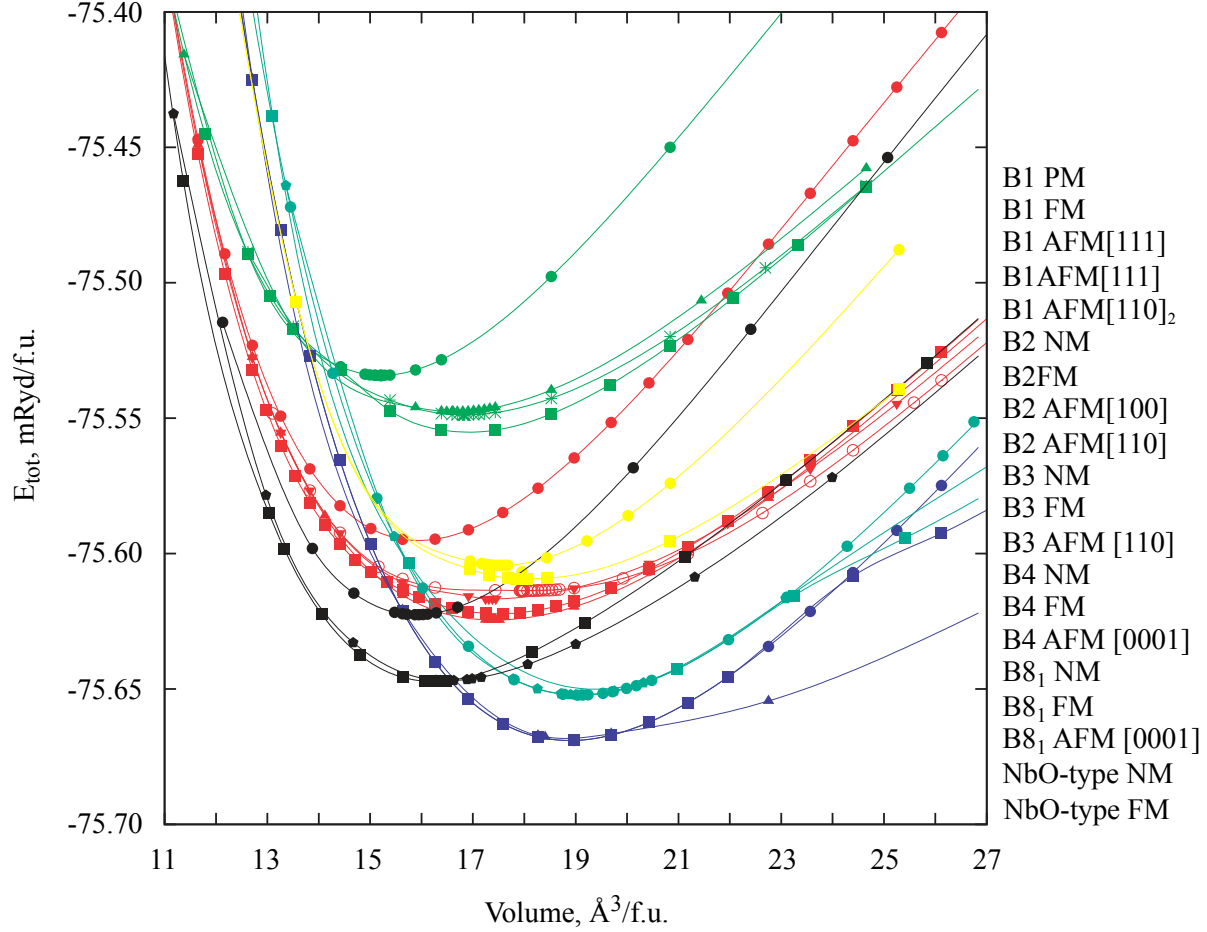


FIG. 1. Total energy versus elementary volume per formula unit for different FeN phases in various magnetic states - nonmagnetic (NM), ferromagnetic (FM) and antiferromagnetic (AFM).

### I. TOTAL ENERGY CALCULATIONS FOR ALL FEN PHASES.

It is clearly seen from the Fig. 1 that the NM ZnS FeN phase has the lowest total energy among others at equilibrium and can be transformed to FM NiAs FeN under pressure.

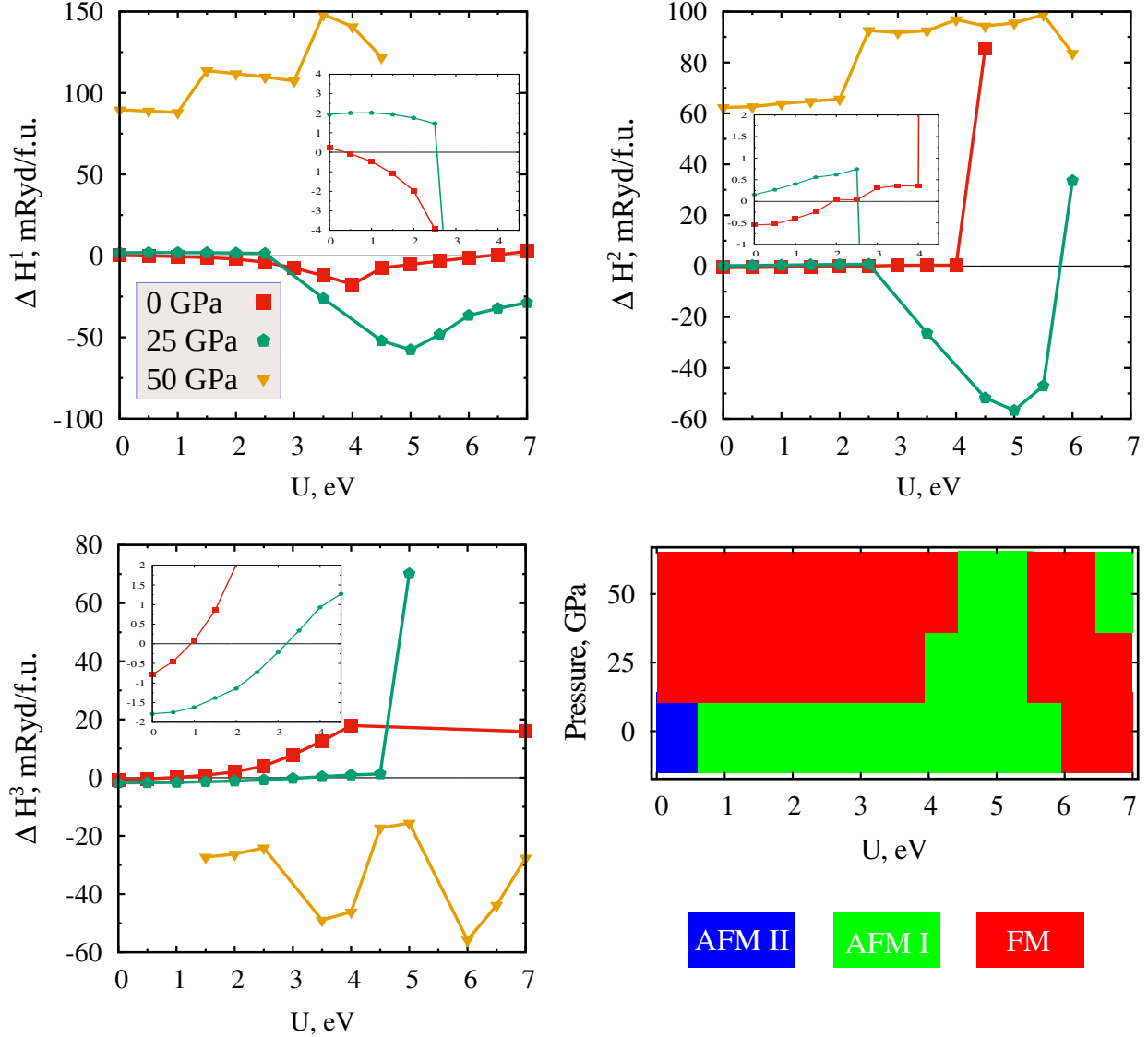


FIG. 2. Enthalpies differences per formula unit between ferromagnetic (FM) and antiferromagnetic (AFM [0001] and AFM [0001]<sub>2</sub>) configurations as a function of on-site Hubbard interaction  $U$  applied to  $d$ -orbitals of iron atoms at different pressure. where  $\Delta H^1 = H(\text{AFM}[0001]_1) - H(\text{FM})$ ,  $\Delta H^2 = H(\text{AFM}[0001]_2) - H(\text{FM})$  and  $\Delta H^3 = H(\text{AFM}[0001]_2) - H(\text{AFM}[0001]_1)$ . The inserts are zoomed graphs for 0-4.5 eV range of  $U$  values. The absence of some data points is due to the convergence problems during the self-consistent calculations.

## II. ENTHALPIES DIFFERENCES FOR THE COMPETITION BETWEEN OF THE FM, AFM [0001] AND AFM[0001]<sub>2</sub> SPIN ARRANGEMENT IN THE MAGNETIC B8<sub>1</sub>.

Enthalpies difference and stability diagram for FM, AFM [0001] and AFM[0001]<sub>2</sub> spin arrangements in the relaxed magnetic B8<sub>1</sub> phase has been computed as a function of on-site Hubbard  $U$

intercalation for three different values of external pressure - 0, 25 and 50 GPa (see Fig. 2). AFM II AFM I denote AFM[0001]<sub>1</sub> and AFM[0001]<sub>1</sub> structure respectively. The AFM[0001]<sub>2</sub> configuration is found to be most favourable for all  $U \lesssim 0.5$  eV at 0 GPa external pressures, while the FM configuration is more preferable than AFM phases for all  $U \lesssim 4.5$  eV for at 25 GPa and 50 GPa pressures. The rest of the diagram has more complicated character and indicate the interplay between FM and AFM exchanges in the magnetic B8<sub>1</sub> phase to be sensitive on the Hubbard  $U$  and external pressure.

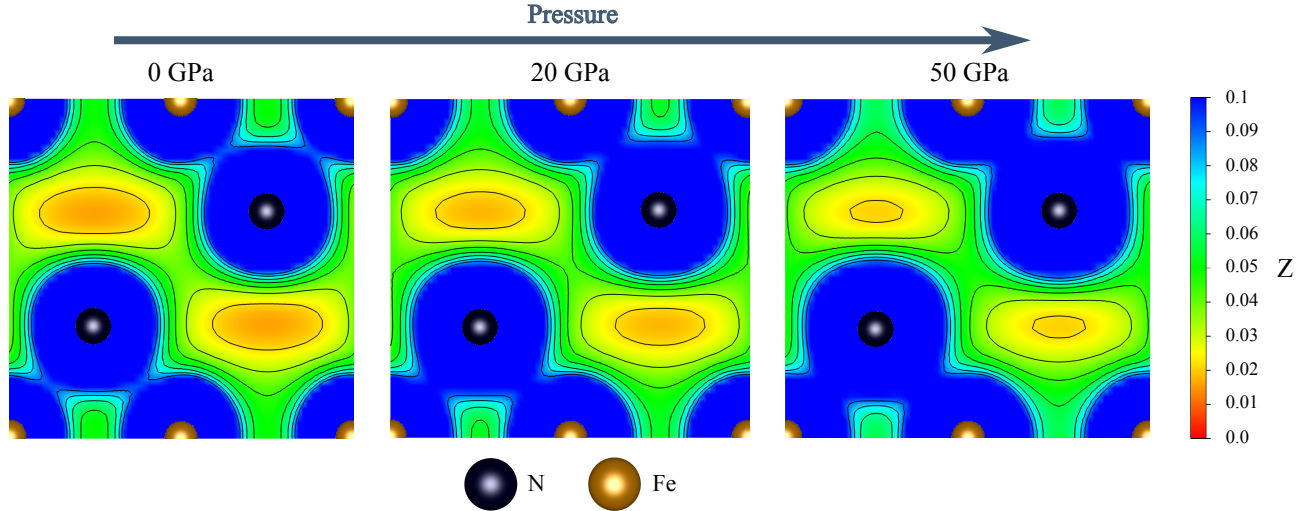


FIG. 3. 2D charge density map evolution during external pressure increasing. The shown charge density map ( $0 < Z < 0.1 e/Bohr^3$ ) correspond to the (012) plane of the primitive  $B8_1$  FeN phase cell. Covalent interaction between Fe and N atoms is clearly visible from the localized valence electrons between the Fe and N atoms and become slightly stronger with pressure.

### III. CHARGE DENSITY AND COVALENT BONDS UNDER THE EXTERNAL PRESSURE.

The charge density map plotted in Fig. 3 confirm the strong covalent characteristics of NiAs FeN. The Fe-N covalent bonding in this phase become stronger with pressure.

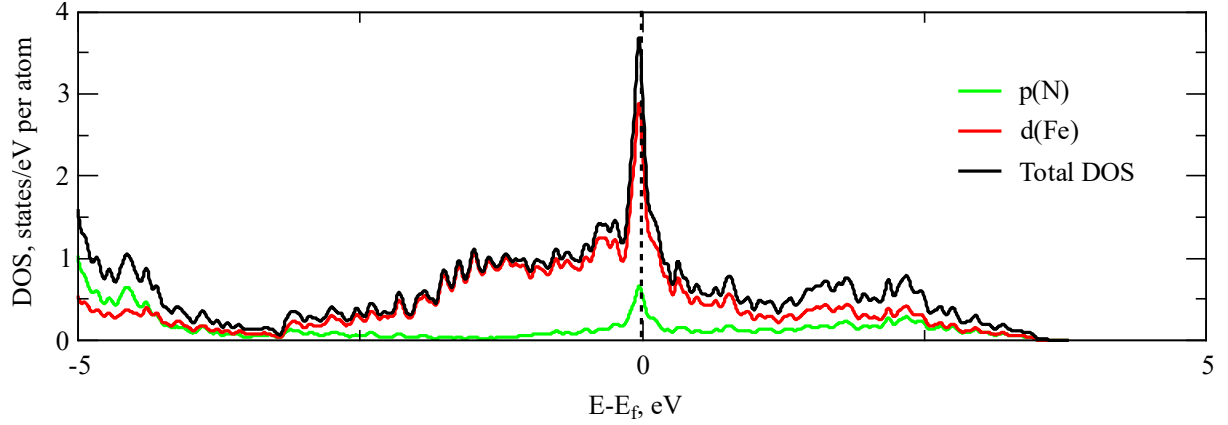


FIG. 4. Density of states and partial density of states for non-magnetic  $B8_1$  FeN phase. Red curve is  $d$ -orbitals contribution of Fe atoms and green curve is  $p$ -orbitals contribution from nitrogen atoms.

#### IV. STONER CRITERIA AND NON-MAGNETIC $B8_1$ FEN PHASE

Due to the  $p(N) - d(Fe)$  orbitals hybridization, the larger value of DOS at Fermi level  $N(E_F)$  together with a band widening emerge at the electronic structure of NM  $B8_1$  FeN phase. So  $1/N(E_F) \gg W$  show that interaction energy is rather higher than the kinetic energy, and thereby favor ferromagnetism and make non-magnetic state unstable.

## V. COHP CALCULATION

The Hamilton-weighted populations were calculated based on periodic plane-wave density-functional theory output with the aid of the Local-Orbital Basis Suite Towards Electronic-Structure Reconstruction software package 'LOBSTER'<sup>?</sup>. With a COHP analysis, it is possible to determine the strength of Fe-N and Fe-Fe bonds of different phases and to understand the bond changes under pressure and during the phase transition. Since  $Fe \uparrow - Fe \downarrow$  bonding of the first coordinate sphere always falls into antibonding regions the AFM coupling is less strength than FM. It is clear that the -ICOHP bond strength of  $Fe - Fe$  bonds for DOWN-spin channel is higher for FM coupling than for AFM, while the UP-channel is stronger for AFM  $Fe - Fe$  bonding. The ICOHP of  $N - N$  is almost independent from the spin arrangement in the FeN structure. Looking to the occupied valence regions of all magnetic FeN structures one can notice a heavy domination of the  $p$  nitrogen levels in a broad energy region, which confirms once again the strong covalency of magnetic FeN.

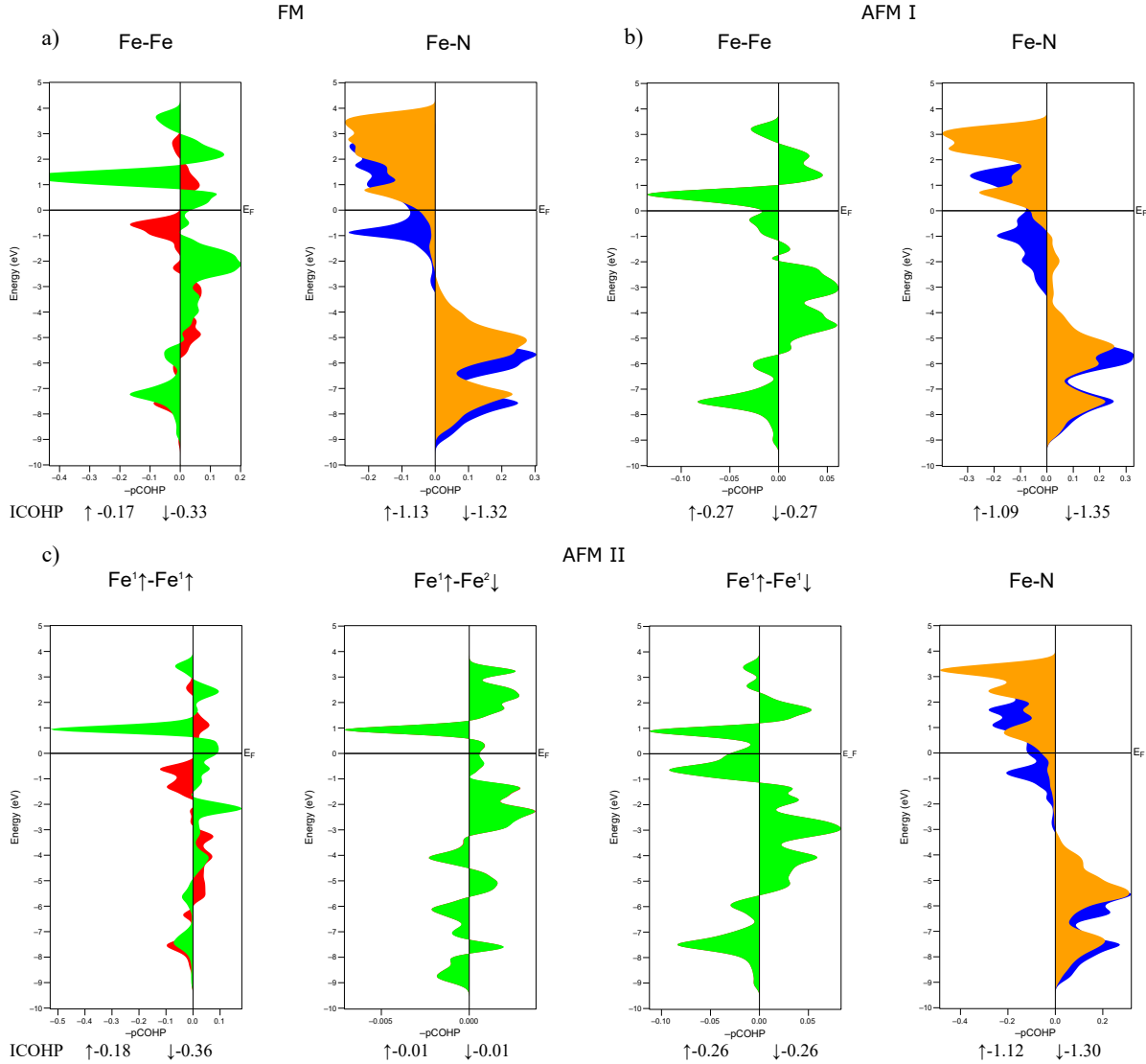


FIG. 5. Calculated crystal orbital Hamilton population (-COHP) for bonding analyses of (a) FM, (b) AFM I (AFM[0001]<sub>1</sub>) and (c) AFM II (AFM[0001]<sub>2</sub>) B8<sub>1</sub> FeN phases - for UP ↑ and DOWN ↓ spin channels separately. Green and red color indicate UP and DOWN spin respectively for  $Fe - Fe$  bonding of the first coordinate sphere (for AFM I structure it correspond to the oppositely polarized iron atoms). Blue and tuscanly colour indicate UP and DOWN spin channel respectively for  $Fe - N$  bonding of the first coordinate sphere. The horizontal line represents the Fermi level  $E_F$ , which is shifted so that it equal to zero. ↑ - ↑ and ↑ - ↓ correspond to the same and oppositely polarized iron atoms. And  $Fe^1 - Fe^1$  and  $Fe^1 - Fe^2$  bonds correspond to iron-iron interaction in the first and second coordinate sphere respectively for the AFM II structure. ICOHP is the integrated -COHP up to the Fermi level for each spin separately. Notice that for ↑ - ↓ bonding UP and DOWN COHPs are equal, thereby green and red colours are superimposed on each other for the AFM bonding.

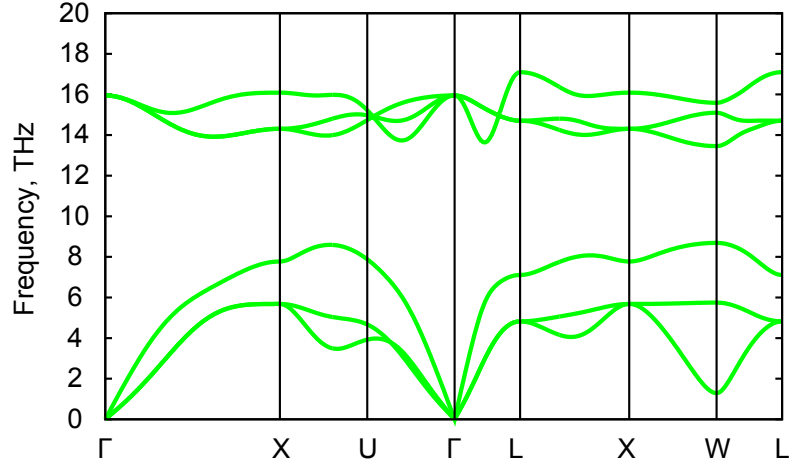


FIG. 6. Phonon spectra for nonmagnetic B3 FeN at the experimental lattice parameter  $a_{B3}^{exp} = 4.335 \text{ \AA}$  .

## VI. DYNAMIC STABILITY OF GROUND STATE FEN PHASE AT ZERO PRESSURE - NM B3 FEN STRUCTURE.

The absence of imaginary modes in phonon spectra for NM B3 FeN phase reveal its stability at experimental lattice parameter  $a_{B3}^{exp} = 4.335 \text{ \AA}$ .

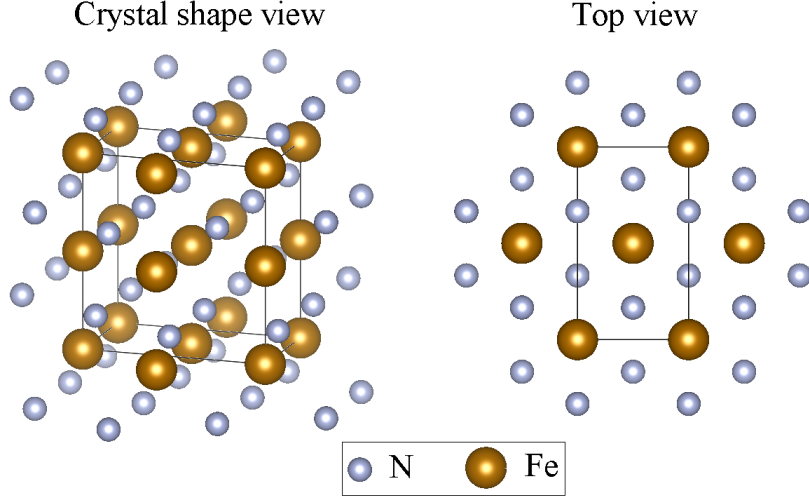


FIG. 7. Rectangular unit cell of FM B8<sub>1</sub> structure used for magnetic exchange calculation.

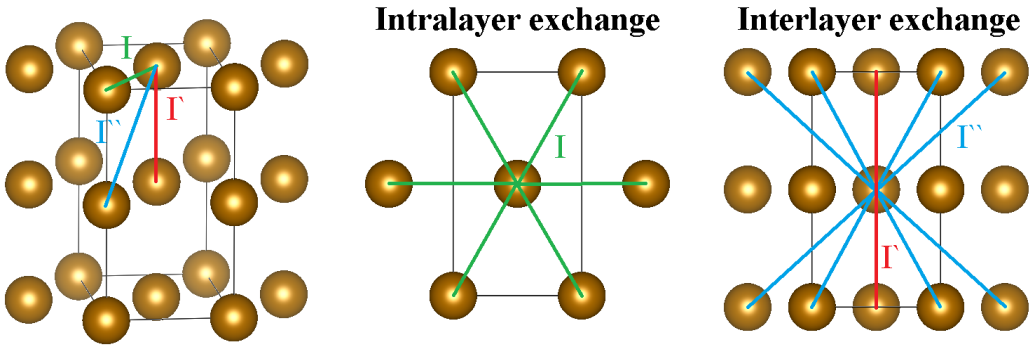


FIG. 8. Intra-layer and inter-layer exchange scheme in the proposed rectangular unit cell of FM B8<sub>1</sub> structure, which correspond to magnetic iron sublattice.

#### A. Critical temperature calculation for FM B8<sub>1</sub> FeN phase.

In order to describe magnetic properties of FM B8<sub>1</sub> FeN we consider here Heisenberg model with an isotropic exchange for one type of the intra-layer first nearest-neighbour exchange (exchange inside hexagonal layers of NiAs-type structure) and two types of the first  $I'$  and the second  $I''$  inter-layer nearest-neighbour exchanges:

$$H = \sum_{\langle i,j \rangle} I \vec{S}_i \vec{S}_j + \sum_{\langle i,j \rangle'} I' \vec{S}_i \vec{S}_j + \sum_{\langle i,j \rangle''} I'' S_i S_j, \quad (1)$$

where  $\vec{S}_i$  and  $\vec{S}_j$  are directions of magnetic moments on the  $i$  and  $j$  metal atoms respectively.

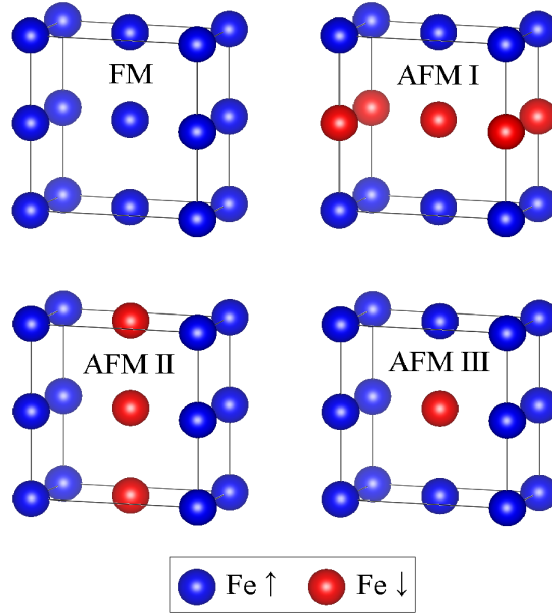


FIG. 9. Four different magnetic configurations used for magnetic exchange calculation between Fe atoms in the framework of DFT: ferromagnetic (FM) and three different anti-ferromagnetic configurations (AFM I, AFM III, AFM III).

Since magnetic Fe atoms of  $B8_1$  structure forms a hexagonal sublattice, in order to implement proposed nearest-neighbour interactions we have to consider an orthorhombic unit cell containing 4 atoms of Fe (see Fig. 7). Therefore using this unit cell magnetic exchanges  $I$ ,  $I'$  and  $I''$  between Fe atoms can be consider in the frame of DFT calculations along with the crystal translation invariance (see Fig. 8).

By performing, the DFT calculations for a crystal with different spin configurations of the magnetic sublattice one can map it onto the model system. Since we do not consider any type of anisotropy, we can stick to collinear DFT calculations for four different unique collinear spin configurations (see Fig. 9): FM - where all the spins allies along the same spin-up direction, AFM I - where one by one hexagonal layers along the  $z$ -direction are oppositely polarized, AFM II - where all the hexagonal layers are identical and 2 atoms are oppositely polarized in each layer of the unit cell, and AFM III - where the only atom in the center of the unit cell has spin-down polarization oppositely to the rest of atoms. Based on the model proposed the following relations of total energies per unit cell for above configurations can be derived:

$$E_{FM} = 24I + 8I' + 48I'' \quad (2)$$

$$E_{AFMI} = 24I - 8I' - 48I'' \quad (3)$$

$$E_{AFMII} = -8I + 8I' - 16I'' \quad (4)$$

$$E_{AFMIII} = 8I \quad (5)$$

$$(6)$$

Since in the framework of DFT the absolute value of total energies has no physical meaning, we have to use the difference between them. So one can take the ferromagnetic state as a reference point and subtract it from other relations. Thereby we can map our model onto DFT results using following relations:

$$\Delta E_{AFMI} = E_{AFMI} - E_{FM} = -16I' - 96I'' \quad (7)$$

$$\Delta E_{AFMII} = E_{AFMII} - E_{FM} = -32I - 64I'' \quad (8)$$

$$\Delta E_{AFMIII} = E_{AFMIII} - E_{FM} = -16I - 8I' - 48I'' \quad (9)$$

By solving this system of linear equations, we can get the following unique solution for values of exchange parameters:

$$I = (\Delta E_{AFMI} - 2\Delta E_{AFMIII})/32 \quad (10)$$

$$I' = (-6\Delta E_{AFMIII} + 3\Delta E_{AFMII} + \Delta E_{AFMI})/32 \quad (11)$$

$$I'' = -(-2\Delta E_{AFMIII} + \Delta E_{AFMII} + \Delta E_{AFMI})/64 \quad (12)$$

For DFT GGA+U calculations with  $U > 0$  eV obtained exchange parameters are lower, thereby it will lower the calculated  $T_C$  value. While using the same formalism for relaxed AFM [0001] structure we computed exchange parameters and got following numbers:  $I = -16.5888$  meV,  $I' = -0.4334$  meV and  $I'' = -0.4007$  meV. Thereby it clear identify the preference of the ferromagnetic order in comparison to AFM [0001] spin arrangement for magnetic B8<sub>1</sub> FeN phase and  $U = 0$  eV.

Based on the proposed model we performed Mote Carlo simulations<sup>7</sup> in "Vampire" atomistic spin dynamics program<sup>7</sup>. A  $50 \times 50 \times 50$  model super-cell with periodic boundary conditions and 32,000 sites was used.

$U$ , eV	$\delta E^1$ , meV	$\delta E^2$ , meV	$\delta E^3$ , meV	Favourable direction
0	0.671	0.656	-0.015	$[11\bar{2}0]$
1	0.840	0.761	-0.080	$[11\bar{2}0]$
2	2.612	2.270	-0.342	$[11\bar{2}0]$
3	0.689	0.735	0.46	$[1\bar{1}00]$
4	-0.160	1.823	1.983	$[1\bar{1}00]$

TABLE I. Magnetic anisotropy at zero pressure as a function of on-site Hubbard  $U$ .  $\delta E^1 = E[0001] - E[11\bar{2}0]$   
 $\delta E^2 = E[0001] - E[1\bar{1}00]$   $\delta E^3 = E[11\bar{2}0] - E[1\bar{1}00]$

## VII. MAGNETIC ANISOTROPY AND EXCHANGES AT ZERO PRESSURE AS A FUNCTION OF ON-SITE HUBBARD $U$ .

Using non-collinear calculations, the magnetic anisotropy energy (MAE) for FM B8<sub>1</sub> FeN phase along three different directions ( $[0001]$ ,  $[11\bar{2}0]$  and  $[1\bar{1}00]$ ) has been computed using the rectangular unit cell. Each magnetic configuration has been relaxed at each  $U$  value and zero pressure. Results clearly indicate the switch of easy-direction for  $U \gtrsim 2$  eV which indicate a complicated behaviour of MAE as a function of  $U$  direction therefore can suggest the non-collinear frustrated in-plane configuration.

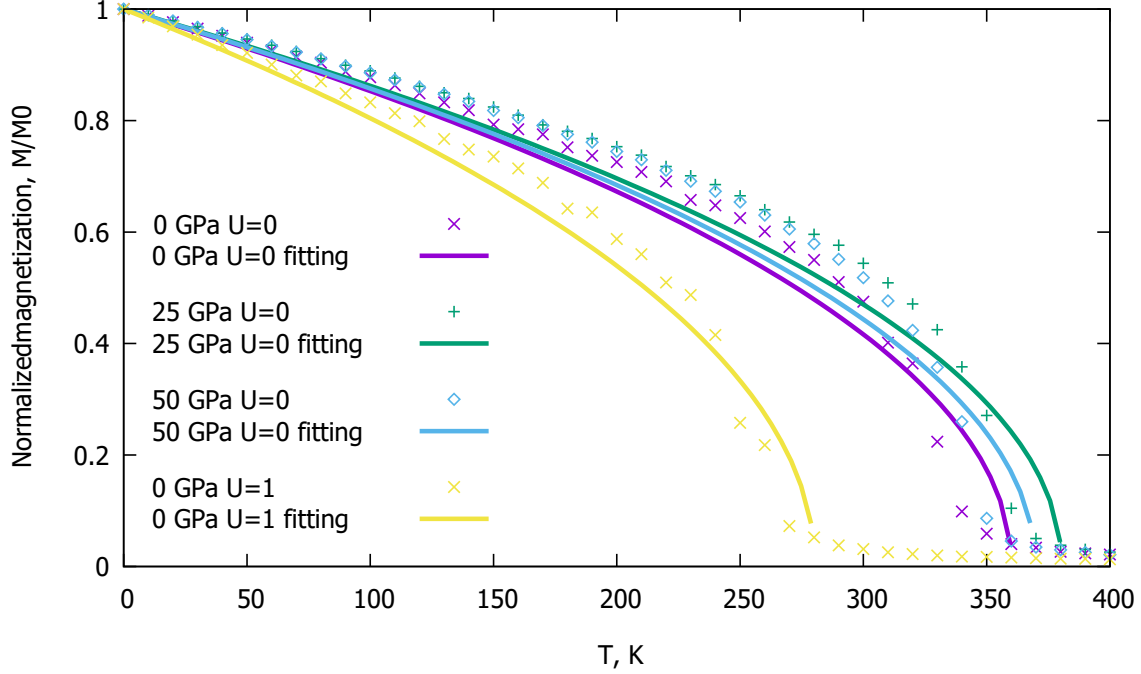


FIG. 10. Monte Carlo simulation of temperature-dependent magnetization for FM B8<sub>1</sub> FeN phase at different pressures and for on-site Hubbard  $U = 1$  eV at 0 GPa (shown by dots). The temperature-dependent magnetization is fitted to the expression  $M^f(T)/M_0 = (1 - T/T_c)^\beta$  (shown by solid lines).

$U$ , eV	$P$ , GPa	$I$ , meV	$I'$ , meV	$I''$ , meV	$T_c$ , K
0	0	-22.17	-16.35	2.24	360
0	25	-21.08	-17.20	1.91	380
0	50	-19.43	-17.51	1.72	370
1	0	-18.52	7.95	-1.52	280
2	0	-20.64	14.96	-1.86	0
3	0	-12.08	43.86	-1.72	0

TABLE II. Magnetic exchanges at different pressures and for different on-site Hubbard  $U$  values.

### VIII. MAGNETIC EXCHANGES AND CURIE TEMPERATURE AT DIFFERENT PRESSURES AND FOR DIFFERENT ON-SITE HUBBARD $U$ VALUES.

Magnetic exchanges  $I$ ,  $I'$  and  $I''$  have been obtained using the collinear spin-polarized calculations for relaxed structures of FM B8<sub>1</sub> FeN phase at each  $U$  value. Zero values of  $T_c$  mean that structure has spin coupling where the anti-ferromagnetic exchange is dominant, and thereby do not exhibit total magnetization at any temperature. It is obvious, that by the increasing  $U$  value the in-plane exchange of second nearest-neighbours switch from the ferromagnetic regime to

anti-ferromagnetic exchange for  $U \gtrsim 1$  eV. And for  $U \gtrsim 2$  eV it has an absolute value which is comparable to the first nearest-neighbour in-plane exchange. Such a competition of comparable FM/AFM exchanges for the first and the second NN should cause spin frustrations.